



Isotopic dependence of the yield ratios of light fragments from different projectiles and their unified neutron skin thicknesses

Ting-Zhi Yan¹ · Shan Li¹

Received: 12 October 2023 / Revised: 4 January 2024 / Accepted: 23 January 2024 / Published online: 3 May 2024
© The Author(s), under exclusive licence to China Science Publishing & Media Ltd. (Science Press), Shanghai Institute of Applied Physics, the Chinese Academy of Sciences, Chinese Nuclear Society 2024

Abstract

The yield ratios of neutron-proton ($R(n/p)$) and ${}^3\text{H}-{}^3\text{He}$ ($R({}^3\text{H}/{}^3\text{He})$) with reduced rapidity from 0 to 0.5 were simulated at 50 MeV/u even-even ${}^{36-56}\text{Ca} + {}^{40}\text{Ca}$, even-even ${}^{48-78}\text{Ni} + {}^{58}\text{Ni}$, and ${}^{100-139}\text{Sn}$ (every third isotopes) + ${}^{112}\text{Sn}$ for full reduced impact parameters using the isospin-dependent quantum molecular dynamics (IQMD) model. The neutron and proton density distributions and root-mean-square radii of the reaction systems were obtained using the Skyrme-Hartree-Fock model, which was used for the phase space initialization of the projectile and target in IQMD. We defined the unified neutron skin thickness as $\Delta R_{np} = \langle r^2 \rangle_n^{1/2} - \langle r^2 \rangle_p^{1/2}$, which was negative for neutron-deficient nuclei. The unified ΔR_{np} values for nuclei with the same relative neutron excess from different isotopic chains were nearly equal, except for extreme neutron-rich isotopes, which is a type of scaling behavior. The yield ratios of the three isotopic chain-induced reactions, which depended on the reduced impact parameter and unified neutron skin thickness, were studied. The results showed that both $R(n/p)$ and $R({}^3\text{H}/{}^3\text{He})$ decreased with a reduced impact parameter for extreme neutron-deficient isotopes; however, they increased with reduced impact parameters for extreme neutron-rich isotopes, and increased with the ΔR_{np} of the projectiles for all reduced impact parameters. In addition, a scaling phenomenon was observed between ΔR_{np} and the yield ratios in peripheral collisions from different isotopic chain projectiles (except for extreme neutron-rich isotopes). Thus, $R(n/p)$ and $R({}^3\text{H}/{}^3\text{He})$ from peripheral collisions were suggested as experimental probes for extracting the neutron or proton skin thicknesses of non-extreme neutron-rich nuclei from different isotopic chains.

Keywords Exotic nuclei · Unified neutron skin thickness · Yield ratios · IQMD

1 Introduction

The exotic nuclei far from the β -stability line have attracted widespread attention because of their special properties, such as extreme N/Z ratios or isospin, significantly different density distributions of neutrons and protons (so-called skin or halo structures), small valence nucleon separation energy, and increased reaction cross-section. Radioactive ion beam facilities have been constructed worldwide to produce exotic nuclei and explore their properties. Classical nuclear

structure models have been continuously developed to comprehensively study their attractive structural characteristics and improve the theoretical nuclear potential and equation of state (EOS). These include the Skyrme-Hartree-Fock (SHF) [1–4], shell model [5–7], relativistic-mean-field [8–11], and so on [12, 13]. One of the most fundamental properties of exotic nuclei is their proton and neutron density distributions. The proton (charge) density distribution can be measured with high accuracy by the elastic electron-scattering and muonic atom X-rays methods [14]. Measurement results of the neutron radius vary significantly owing to the complex strong interaction between nucleons, including the hadron scattering [15–17], giant dipole resonance [18, 19], and antiprotonic atoms methods [20–22]. Some of the experimental probes are unsuitable for unstable nuclei; therefore, studies on nuclei radii primarily focus on stable nuclei or nuclei close to β -stability. Some isospin-dependent quantities from nuclear reactions, such as collective flows

This work was supported by National Natural Science Foundation of China (No. 11405025).

✉ Ting-Zhi Yan
ytz0110@163.com

¹ School of Energy and Power Engineering, Northeast Electric Power University, Jilin 132012, China

[23–30], yield ratios of neutron-proton [31–39], and ${}^3\text{H}/{}^3\text{He}$ [39, 40], have been studied to explore the isospin physics such as the symmetry energy [41, 42] and nucleon-nucleon cross section [43]. We used the neutron skin thickness (defined as the difference between the root-mean-square (rms) radii of the neutron and proton, i.e., $\Delta R_{\text{np}} = \langle r^2 \rangle_{\text{n}}^{1/2} - \langle r^2 \rangle_{\text{p}}^{1/2}$), which was calculated using the SHF method, and explored the yield ratios of neutron/proton and ${}^3\text{H}/{}^3\text{He}$ within projectile-like rapidities from different Ca isotopic projectiles (the collisions were simulated in the framework of isospin-dependent quantum molecular dynamics (IQMD) model using nucleon density distributions from SHF above for phase initialization of Ca projectiles) dependent on the neutron skin thicknesses of Ca projectiles, which show linearly increasing correlations between them [44]. Similar correlations were studied for the proton skin thicknesses of neutron-deficient Ni isotopes that exhibited exponentially declining relationships [45], where the proton skin thickness was defined as $\Delta R_{\text{pn}} = \langle r^2 \rangle_{\text{p}}^{1/2} - \langle r^2 \rangle_{\text{n}}^{1/2}$. In this work, we used the unified neutron skin thickness ($\Delta R_{\text{np}} = \langle r^2 \rangle_{\text{n}}^{1/2} - \langle r^2 \rangle_{\text{p}}^{1/2}$) to combine the neutron skin thickness and the proton skin thickness, such that the ΔR_{np} of a neutron-deficient nucleus was negative in that case. The unified neutron skin thickness dependence of the yield ratios of the neutron-proton and ${}^3\text{H}-{}^3\text{He}$ was studied for Ca, Ni, and Sn isotopic projectiles, and the reduced impact parameter dependence for the above correlation was also explored.

2 Method

The neutron and proton density distributions and nuclear radii of the projectiles and targets were extracted using the SHF theory with the so-called SkM* parameters [46]. These were then used in the IQMD model to generate the phase space of the projectile and target. The proper phase space must be correctly selected according to the experimental average binding energy and rms radius. The time-evolution stability of the phase space should be carefully examined to avoid large fluctuations in the average binding energy and rms radius. The selected phase space should have a small fluctuation in the rms radius, particularly in the first several dozen fm/c and for nuclei far from the β -stability line. Using these carefully selected initialization phase spaces of the projectile and target as input files, further time evolution of the reaction was performed within the framework of the IQMD model, which is based on the general QMD model [47].

The nuclear mean-field potential used in the IQMD model can be parameterized as follows:

$$U(\rho, \tau_z) = \alpha \left(\frac{\rho}{\rho_0} \right) + \beta \left(\frac{\rho}{\rho_0} \right)^\gamma + \frac{1}{2} (1 - \tau_z) V_c + C_{\text{sym}} \frac{(\rho_{\text{n}} - \rho_{\text{p}})}{\rho_0} \tau_z + U^{\text{Yuk}}, \quad (1)$$

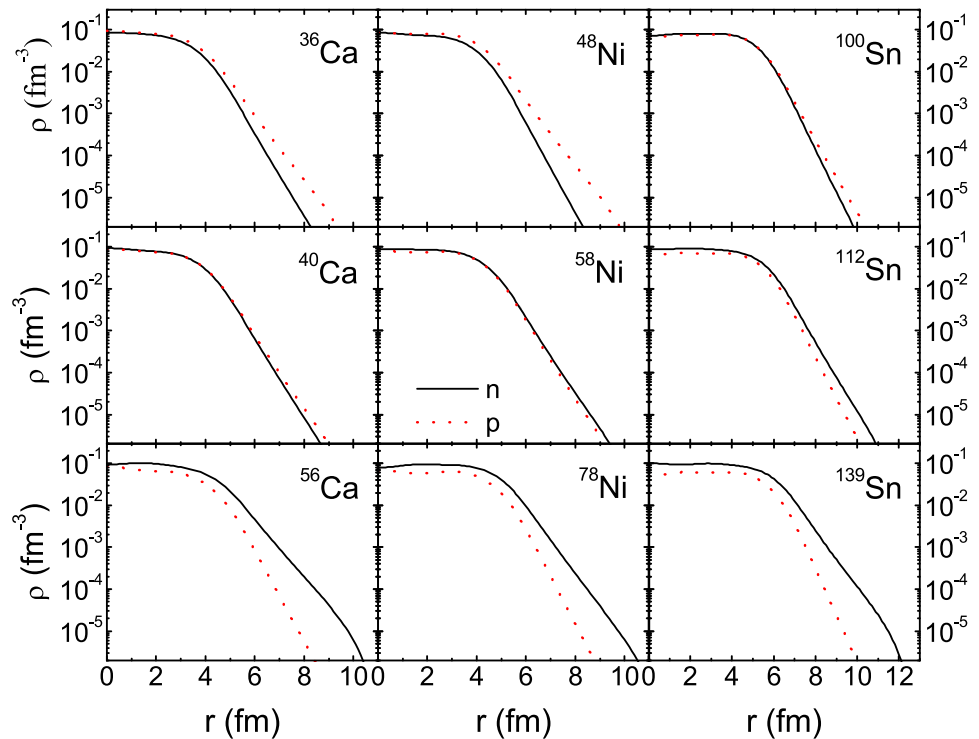
where ρ_0 is the normal nuclear matter density (0.16 fm^{-3}); ρ , ρ_{p} , ρ_{n} are the total, proton, and neutron densities, respectively; and τ_z is the z th constituent of the isospin degree of freedom, which is equal to 1 or -1 for neutrons or protons, respectively. The parameters α , β , and γ represent the different nuclear equations of state. C_{sym} is the symmetry energy strength owing to the asymmetry of neutrons and protons in the nucleus. $C_{\text{sym}} = 32 \text{ MeV}$ was used in this study. V_c and U^{Yuk} denote the Coulomb and Yukawa (surface) potentials, respectively. We used $\alpha = -356 \text{ MeV}$, $\beta = 303 \text{ MeV}$, and $\gamma = 1.17$, which correspond to the so-called soft EOS with an incompressibility of $K = 200 \text{ MeV}$. Although a soft EOS was used without momentum-dependent interactions and yield of fragments was affected, the yield ratio remained relatively unchanged.

In this study, the reduced impact parameters of collisions of even-even ${}^{36-56}\text{Ca} + {}^{40}\text{Ca}$, even-even ${}^{48-78}\text{Ni} + {}^{58}\text{Ni}$, and ${}^{100-139}\text{Sn}$ (every third isotope) + ${}^{112}\text{Sn}$ at 50 MeV/u were simulated using the IQMD model with the soft EOS parameterization. The reduced impact parameter is defined as $b_{\text{re}} = b/b_{\text{max}}$, where b_{max} is the sum of the radii of the target and projectile. The yields of light fragments were restricted within projectile-like midrapidity; therefore, the reduced rapidity of the fragments ($y = (y/y_{\text{p}})_{\text{c.m.}}$, where y_{p} is the projectile rapidity) was between 0 and 0.5 to ensure that the fragments originated from the projectile. The yield ratios of neutron-proton ($R(n/p)$) and ${}^3\text{H}-{}^3\text{He}$ ($R({}^3\text{H}/{}^3\text{He})$) were calculated using the yields of neutrons, protons, ${}^3\text{H}$, and ${}^3\text{He}$. The yields of the light particles were accumulated from 160 to 200 fm/c to improve statistics.

3 Results and discussion

The normalized neutron and proton density distributions of typical neutron-deficient, stable, and neutron-rich isotopes of Ca, Ni, and Sn obtained using the SHF method with the SkM* parameters are shown in Fig. 1. The proton skin and neutron skin structures are evident in the neutron-deficient and neutron-rich nuclei of medium-mass Ca and Ni, respectively, whereas the proton skin structure is difficult to form in the relatively heavier element Sn owing to the Coulomb potential, as we have already realized. The nuclear radii of the isotopes of the three elements (Ca, Ni, and Sn) related to their nuclear mass numbers are shown in the left panel of Fig. 2. The squares and circles represent the rms radii of neutrons and protons, respectively. The solid and dotted

Fig. 1 (Color online) Normalized neutron (solid lines) and proton (dashed lines) density distributions of $^{36,40,56}\text{Ca}$, $^{48,58,78}\text{Ni}$, and $^{100,112,139}\text{Sn}$ calculated using SkM* parametrization of the SHF method



lines indicate the results for even-even Ca with the RCHB method [48] and Ni and Sn with the deformed self-consistent mean-field Skyrme HF+BCS method [49], which are close to our results for Ni and Sn but deviate significantly for the proton density of Ca. The calculated unified neutron skin thicknesses of Ca, Ni, and Sn, based on the simulated neutron and proton radii, are shown in the right panel of Fig. 2. The upward triangles and solid lines are our SHF results and the theoretical results from the aforementioned studies, respectively, while the downward triangles are experimental values of these three nuclei extracted from Ref. [50] obtained using the antiproton atoms method. Our simulated ΔR_{np} closely matched those of other studies, except for extremely neutron-rich Ca, and were within the error bars of the experimental values. The experimental data for the Sn isotopes measured using other methods were also compared with the model results in Ref. [49] and were consistent with experimental results within the error ranges.

Reference [50] demonstrated the existence of an approximate linear correlation between the experimental value of the neutron skin thickness of 26 stable nuclei and their relative neutron excess I ($I = (N - Z)/A$). We present the same correlation for the Ca, Ni, and Sn isotopes in Fig. 3. The simulated unified neutron skin thickness with the SHF theory increases linearly with the relative neutron excess, except for those of extreme neutron-rich nuclei, and the curves for the three isotopic chains almost overlap, except for those of extreme neutron-rich isotopes. This suggests the possibility of scaling behavior for different isotope chains

for the correlation. This interesting phenomenon can further elucidate the EOS of asymmetric nuclear matter [51], and more accurate theoretical calculations and experimental data on the unified neutron skin thickness of isotope chains are required.

The extracted projectile-like yield ratios $R(n/p)$ (left panels) and $R(^3\text{H}/^3\text{He})$ (right panels) from the Ca (upper panels), Ni (middle panels), and Sn (bottom panels) isotopic projectiles within different reduced impact parameters are shown in Fig. 4. Approximately half of the isotopes are shown in the figure to illustrate the changing trend more clearly. The values of $R(n/p)$ and $R(^3\text{H}/^3\text{He})$ from different b_{re} are different. They decrease with increasing b_{re} for extreme proton-rich isotopes, and gradually change to exhibit an increasing trend with the b_{re} with the growing constituent neutron-proton ratio (N/Z) of the projectile isotopes. Furthermore, larger values at the same b_{re} correspond to projectiles with larger N/Z . The fragments at $0 < y < 0.5$ are emitted from the projectile in the overlap zone of the collision, and their constituent neutron-proton ratios should be close to that of the projectile. However, as the proton or neutron skin structure plays an increasingly important role with increasing collision parameters, the N/Z of the projectile-like fragment and the yield ratios of $R(n/p)$ and $R(^3\text{H}/^3\text{He})$ vary accordingly. Thus, the skin structure can affect the yield ratios, and therefore, the unified neutron skin thickness dependence of the yield ratios from different reduced impact parameters for Ca (upper panels), Ni (middle panels), and Sn (lower panels) are examined in Fig. 5. The yield ratios $R(n/p)$

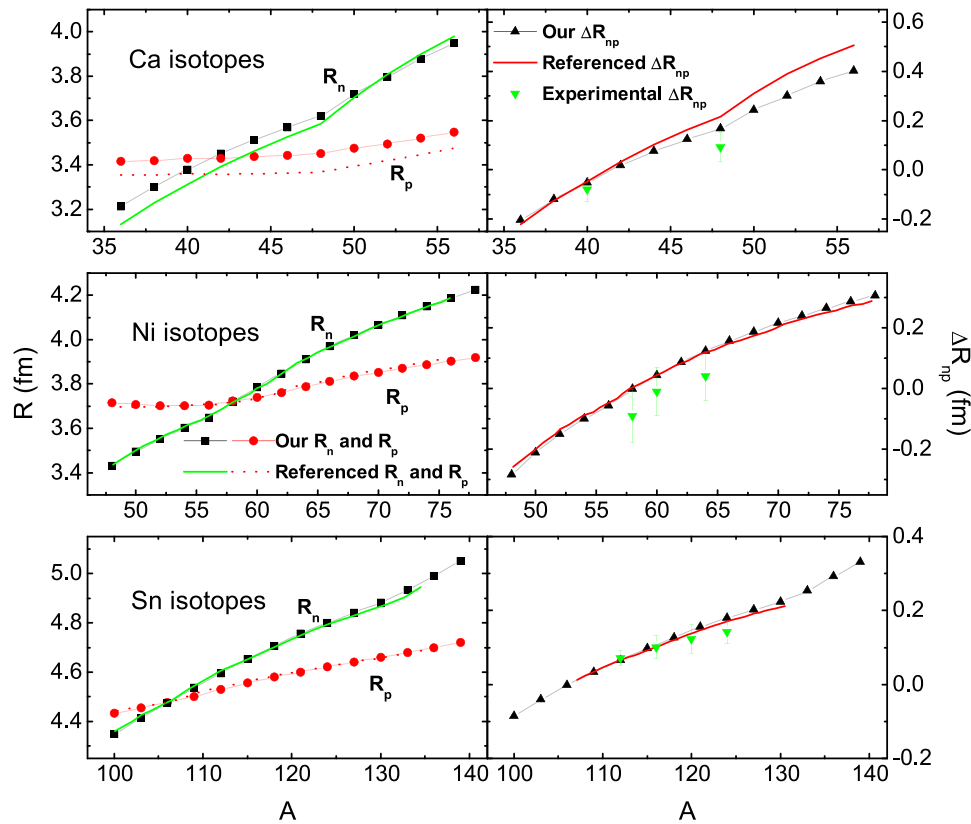


Fig. 2 (Color online) Left panel: Mass number dependence of the rms radii of neutrons (line + square) and protons (line + circle) (left panel) of even-even $^{36-56}\text{Ca}$, even-even $^{48-78}\text{Ni}$, and $^{100-139}\text{Sn}$ (every third isotope) calculated using SkM* parametrization of the SHF method. The solid and the dotted lines are the referenced results for neutrons and protons, respectively, in which even-even Ca isotopes are taken from Ref. [48] calculated with relativistic continuum Hartree-Bogoliubov (RCHB) theory. The even-even Ni and Sn isotopes

are extracted from Ref. [49] in the framework of the deformed self-consistent mean-field Skyrme HF+BCS method. Right panel: Same as left panel but for the unified neutron skin thickness. The upward triangles are our SHF results; the solid lines are the calculated results based on the referenced neutron and proton rms radii of the left panel; and the downward triangles are the experimental values extracted from Ref. [50]

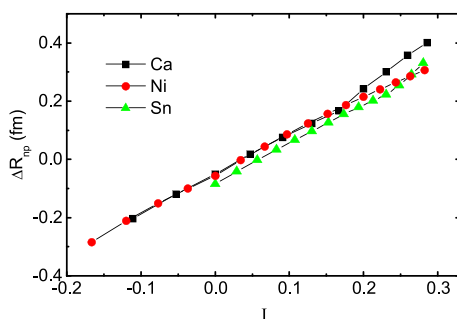


Fig. 3 (Color online) Relative neutron excess dependence of the unified neutron skin thickness simulated for the Ca (squares), Ni (circles), and Sn (triangles) isotopes

and $R(^3\text{H}/^3\text{He})$ from all the reduced impact parameters both increase with the unified neutron skin thickness ΔR_{np} in a monotonic but nonlinear manner, and the increase is faster

for larger reduced impact parameters. The corresponding nuclei with equal yield ratios can also be easily obtained from different reduced impact parameters. The left panel of Fig. 5 indicates that ^{40}Ca , ^{60}Ni , and ^{118}Sn have equal yield ratios $R(n/p)$ for different reduced impact parameters, and they are near the β stability line. As shown in the right-hand panel of Fig. 5, ^{50}Ni and ^{106}Sn have equal $R(^3\text{H}/^3\text{He})$, which are neutron-rich nuclei with smaller N/Z than those obtained from $R(n/p)$. The Ca isotope with equal $R(^3\text{H}/^3\text{He})$ from different reduced impact parameters is beyond the Ca scope we studied; however, it is definitely neutron-rich.

Figures 6 and 7 compare the isotopic chains of the projectile-like yield ratios $R(n/p)$ and $R(^3\text{H}/^3\text{He})$ from different reduced impact parameters that depend on the unified neutron skin thickness ΔR_{np} of the projectile. Differences are observed in the yield ratios among the three isotopic systems in central and semi-peripheral collisions, especially for Sn projectiles. However, in peripheral collisions, the yield ratios from the three isotopic systems almost overlap with

Fig. 4 (Color online) Yield ratios of $R(n/p)$ (left panels) and $R(^3\text{H}/^3\text{He})$ (right panels) with $0 < y < 0.5$ as a function of the reduced impact parameter from some isotopes of even-even $^{36-56}\text{Ca} + ^{40}\text{Ca}$, even-even $^{48-78}\text{Ni} + ^{58}\text{Ni}$, and $^{100-139}\text{Sn}$ (every third isotope) + ^{112}Sn at 50 MeV/u simulated using the IQMD model with soft-EOS parameterization

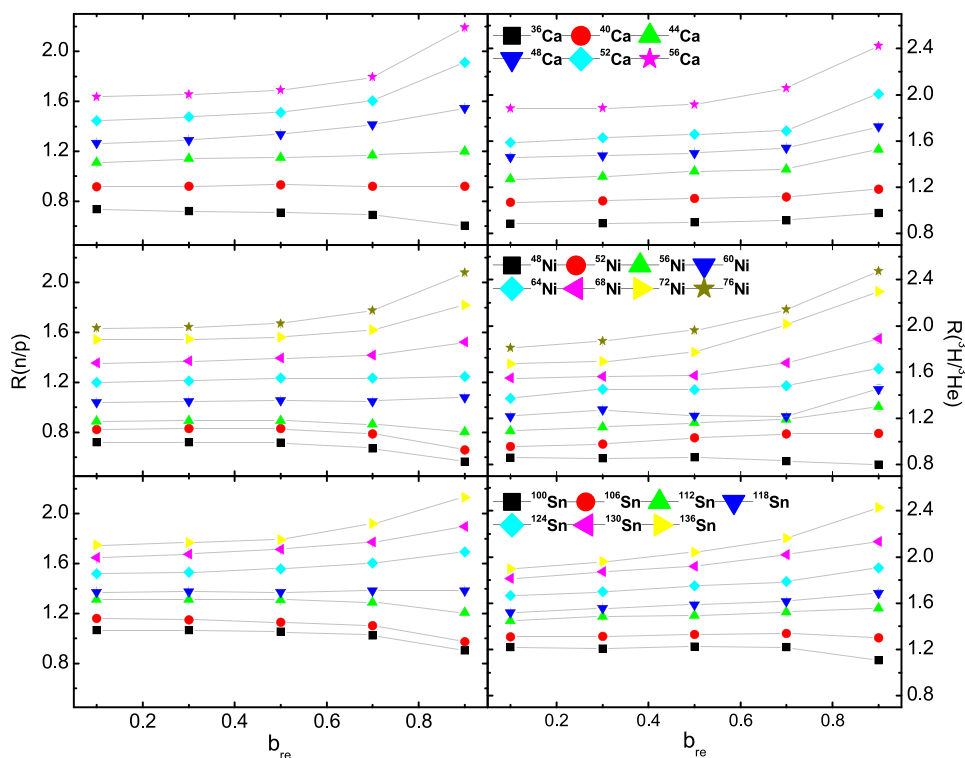


Fig. 5 (Color online) Similar to Fig. 4 but for the unified neutron skin thickness ΔR_{np} dependence

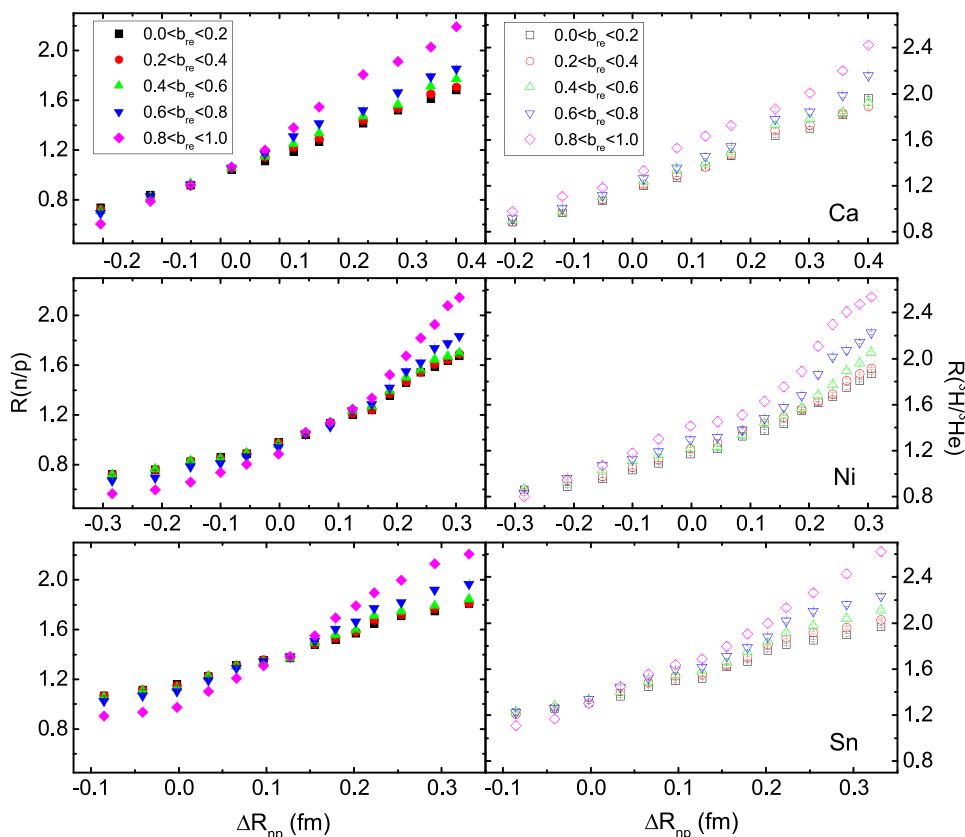


Fig. 6 (Color online) Isotopic chains comparison of the yield ratio $R(n/p)$ at $0 < y < 0.5$ from different reduced impact parameters as the function of the unified neutron skin thickness ΔR_{np}

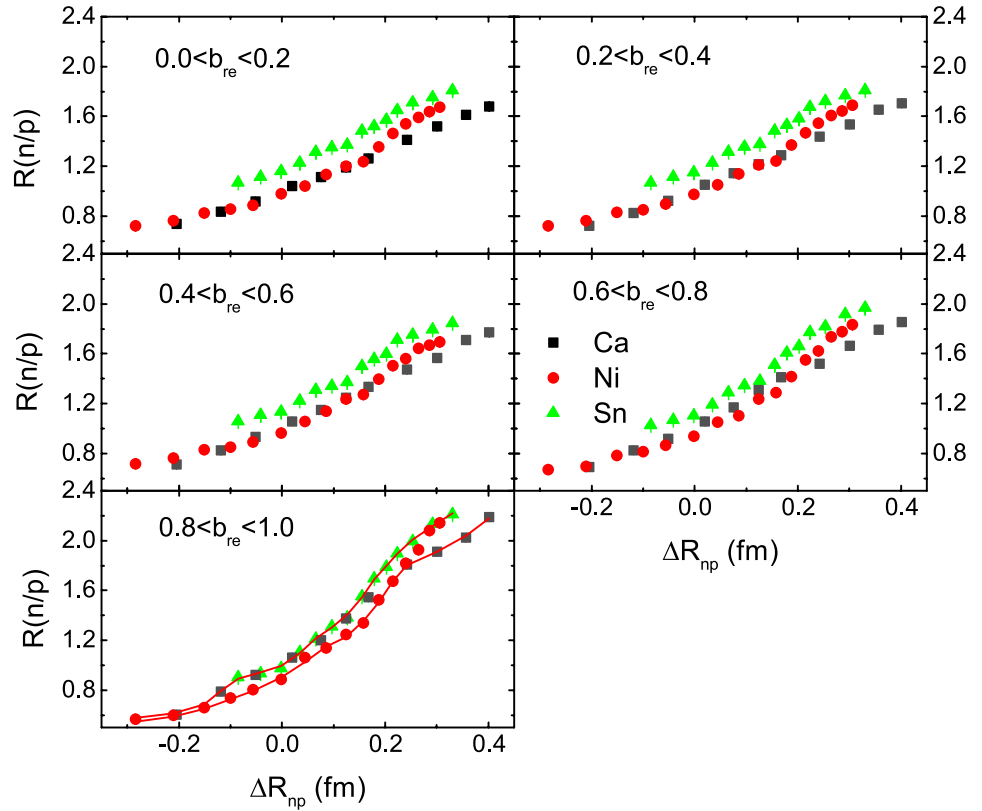
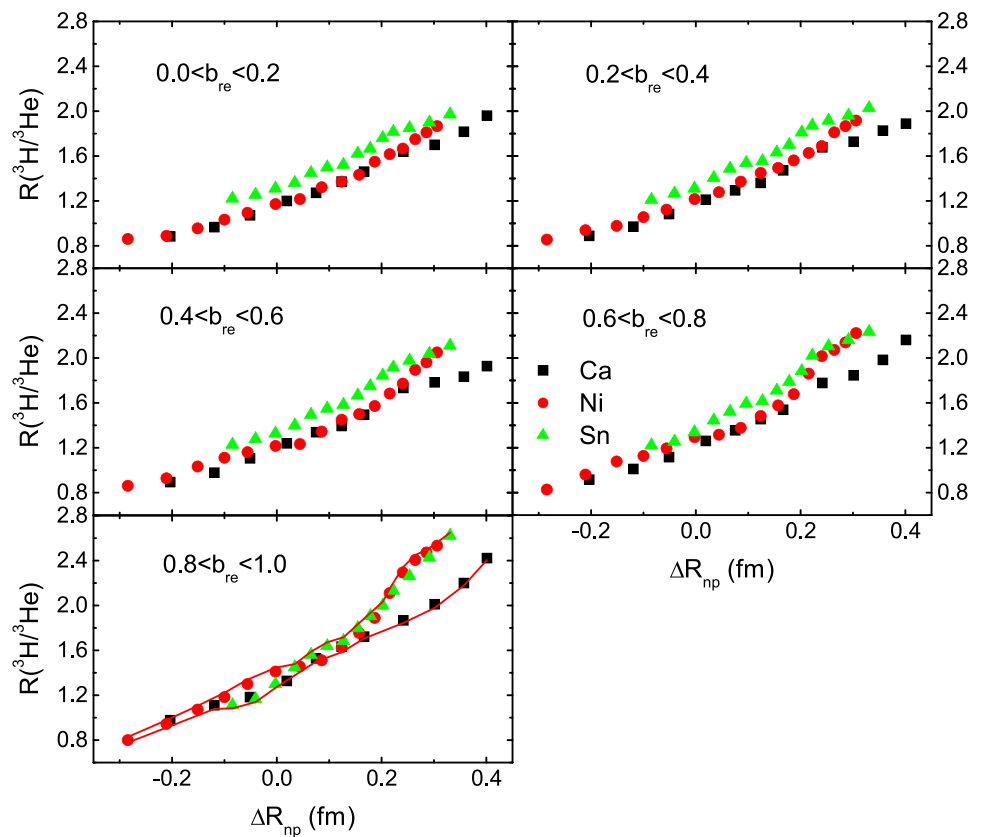


Fig. 7 (Color online) Similar to Fig. 6 but for the yield ratio $R(^3\text{H}/^3\text{He})$



each other, except for several extreme neutron-rich Ca isotopes. This may be due to the inaccurate neutron skin thickness of extreme neutron-rich light Ca isotopes calculated using the same set of theoretical parameters. Thus, a scaling behavior may exist for different isotopic chains (except for extreme neutron-rich isotopes) between the projectile-like light fragment yield ratios from the peripheral reactions and the unified neutron skin thickness of the projectile. In other words, nuclei with the same unified neutron skin thickness would produce the same $R(n/p)$ and $R(^3\text{H}/^3\text{He})$ from peripheral collisions. The scaling behavior can be used to extract the unified neutron skin thickness (including neutron-rich or neutron-deficient isotopes) of an isotope by experimentally observing the mid-rapidity yield ratios of $R(n/p)$ or $R(^3\text{H}/^3\text{He})$ in the peripheral reactions from the isotopes of other elements. The enveloping curves for $R(n/p)$ and $R(^3\text{H}/^3\text{He})$ for the three isotopic chains from peripheral reactions are plotted in Figs. 6 and 7 to show the estimated range of skin sizes extracted for one isotope from $R(n/p)$ or $R(^3\text{H}/^3\text{He})$ of the three isotopic chains.

4 Summary

The projectile-like yield ratios $R(n/p)$ and $R(^3\text{H}/^3\text{He})$ were studied for even-even $^{36-56}\text{Ca} + ^{40}\text{Ca}$, even-even $^{48-78}\text{Ni} + ^{58}\text{Ni}$, and $^{100-139}\text{Sn}$ (every third isotope) + ^{112}Sn at 50 MeV/u simulated using the IQMD model with the sampled initial nucleon densities by applying the SHF method. The yield ratios decreased with the increasing reduced impact parameter for extreme neutron-deficient isotopes, and then gradually increased with the reduced impact parameter for extreme neutron-rich isotopes. The yield ratios from different reduced impact parameters for isotropic projectiles monotonically increased with the unified neutron skin thickness ΔR_{np} of the projectile. Scaling behaviors may exist between the unified ΔR_{np} and the relative neutron excess for different isotopic chains, and between the unified ΔR_{np} of the projectile and the projectile-like light fragments' yield ratios from peripheral reactions. In other words, the yield ratios at the same ΔR_{np} but from different projectiles are the same; therefore, $R(n/p)$ and $R(^3\text{H}/^3\text{He})$ can be used as experimental probes to extract the unified ΔR_{np} for different isotopic chains and deduce information about isospin dependent nuclear potential and EOS. The proton and neutron densities and distribution radii were calculated using the SkM* parameters of SHF in our work, whereas the initialization and propagation of the nuclei were performed with a different mean-field potential of the transport model, which altered ΔR_{np} and even $R(n/p)$ and $R(^3\text{H}/^3\text{He})$. Therefore, further precise theoretical and experimental studies are required to investigate this scaling phenomenon.

Author Contributions All authors contributed to the study conception and design. Material preparation, data collection and analysis were performed by SL. The first draft of the manuscript was written by T-ZY and all authors commented on previous versions of the manuscript. All authors read and approved the final manuscript.

Data availability statement The data that support the findings of this study are openly available in Science Data Bank at <https://cstr.cn/31253.11.sciencedb.16034> and <https://doi.org/10.57760/sciencedb.16034>.

Declarations

Conflict of interest The authors declare that they have no Conflict of interest.

References

1. C.J. Horowitz, S.J. Pollock, P.A. Souder et al., Parity violating measurements of neutron densities. *Phys. Rev. C* **63**, 025501 (2001). <https://doi.org/10.1103/PhysRevC.63.025501>
2. P. Danielewicz, Surface symmetry energy. *Nucl. Phys. A* **727**, 233–268 (2003). <https://doi.org/10.1016/j.nuclphysa.2003.08.001>
3. M. Liu, N. Wang, Z.X. Li et al., Neutron skin thickness of nuclei and effective nucleon-nucleon interactions. *Chin. Phys. Lett.* **23**(4), 804 (2006). <https://doi.org/10.1088/0256-307X/23/4/012>
4. E.B. Huo, K.R. Li, X.Y. Qu et al., Continuum Skyrme Hartree-Fock-Bogoliubov theory with Green's function method for neutron-rich Ca, Ni, Zr, and Sn isotopes. *Nucl. Sci. Tech.* **34**(7), 105 (2023). <https://doi.org/10.1007/s41365-023-01261-9>
5. K. Bennaceur, F. Nowacki, J. Okolowicz et al., Study of the $^7\text{Be}(p, \gamma)^8\text{B}$ and $^7\text{Li}(n, \gamma)^8\text{Li}$ capture reactions using the shell model embedded in the continuum. *Nucl. Phys. A* **651**, 289–319 (1999). [https://doi.org/10.1016/S0375-9474\(99\)00133-5](https://doi.org/10.1016/S0375-9474(99)00133-5)
6. K. Kaneko, Y. Sun, G. de Angelis, Enhancement of high-spin collectivity in $N=Z$ nuclei by the isoscalar neutron-proton pairing. *Nucl. Phys. A* **957**, 144–153 (2017). <https://doi.org/10.1016/j.nuclphysa.2016.08.007>
7. Z.H. Sun, Q. Wu, Z.H. Zhao et al., Resonance and continuum Gamow shell model with realistic nuclear forces. *Phys. Lett. B* **769**, 227–232 (2017). <https://doi.org/10.1016/j.physletb.2017.03.054>
8. Z.J. Wang, Z.Z. Ren, Elastic electron scattering on exotic light proton-rich nuclei. *Phys. Rev. C* **70**, 034303 (2004). <https://doi.org/10.1103/PhysRevC.70.034303>
9. S. Yoshida, H. Sagawa, Neutron skin thickness and equation of state in asymmetric nuclear matter. *Phys. Rev. C* **69**, 024318 (2004). <https://doi.org/10.1103/PhysRevC.69.024318>
10. A. Bhagwat, Y.K. Gambhir, Recently measured reaction cross sections with low energy fp-shell nuclei as projectiles: Microscopic description. *Phys. Rev. C* **73**, 054601 (2006). <https://doi.org/10.1103/PhysRevC.73.054601>
11. J.G. Chen, X.Z. Cai, H.Y. Zhang et al., Proton halo or skin in the excited states of light nuclei. *Chin. Phys. Lett.* **20**(7), 1021 (2003). <https://doi.org/10.1088/0256-307X/20/7/314>
12. C.W. Ma, Y.P. Liu, H.L. Wei et al., Determination of neutron-skin thickness using configurational information entropy. *Nucl. Sci. Tech.* **33**(1), 6 (2022). <https://doi.org/10.1007/s41365-022-00997-0>
13. X.X. Sun, S.G. Zhou, Deformed halo nuclei and shape decoupling effects. *Nucl. Tech. (in Chinese)* **46**(08), 080015 (2023). <https://doi.org/10.11889/j.0253-3219.2023.hjs.46.080015>

14. I. Angeli, A consistent set of nuclear rms charge radii: properties of the radius surface $R(N, Z)$. *At. Data Nucl. Data Tables* **87**, 185–206 (2004). <https://doi.org/10.1016/j.adt.2004.04.002>
15. L. Ray, W.R. Coker, G.W. Hoffmann et al., Uncertainties in neutron densities determined from analysis of 0.8 GeV polarized proton scattering from nuclei. *Phys. Rev. C* **18**, 2641 (1978). <https://doi.org/10.1103/PhysRevC.18.2641>
16. S. Terashima, H. Sakaguchi, H. Takeda et al., Proton elastic scattering from tin isotopes at 295 MeV and systematic change of neutron density distributions. *Phys. Rev. C* **77**, 024317 (2008). <https://doi.org/10.1103/PhysRevC.77.024317>
17. A. Tamii, I. Poltoratska, P. von Neumann-Cosel et al., Complete electric dipole response and the neutron skin in ^{208}Pb . *Phys. Rev. Lett.* **107**, 062502 (2011). <https://doi.org/10.1103/PhysRevLett.107.062502>
18. A. Krasznahorkay, J. Bacelar, J.A. Bordewijk et al., Excitation of the isovector giant dipole resonance by inelastic α scattering and the neutron skin of nuclei. *Phys. Rev. Lett.* **66**, 1287 (1991). <https://doi.org/10.1103/PhysRevLett.66.1287>
19. M. Csatlós, A. Krasznahorkaya, D. Sohler et al., Measurement of neutron-skin thickness in ^{208}Pb by excitation of the GDR via inelastic α -scattering. *Nucl. Phys. A* **719**, C304–C307 (2003). [https://doi.org/10.1016/S0375-9474\(03\)00937-0](https://doi.org/10.1016/S0375-9474(03)00937-0)
20. P. Lubinski, J. Jastrzqbski, A. Grochulska et al., Neutron halo in heavy nuclei from antiproton absorption. *Phys. Rev. Lett.* **73**, 3199 (1994). <https://doi.org/10.1103/PhysRevLett.73.3199>
21. R. Schmidt, F.J. Hartmann, T. von Egidy et al., Nucleon density of ^{172}Yb and ^{176}Yb at the nuclear periphery determined with antiprotonic x rays. *Phys. Rev. C* **58**, 3195 (1998). <https://doi.org/10.1103/PhysRevC.58.3195>
22. B. Kłos, A. Trzcińska, J. Jastrzqbski et al., Neutron density distributions from antiprotonic ^{208}Pb and ^{209}Bi atoms. *Phys. Rev. C* **76**, 014311 (2007). <https://doi.org/10.1103/PhysRevC.76.014311>
23. B.A. Li, C.M. Ko, Isospin dependence of collective flow. *Nucl. Phys. A* **654**, 797c–802c (1999). [https://doi.org/10.1016/S0375-9474\(00\)88549-8](https://doi.org/10.1016/S0375-9474(00)88549-8)
24. L.W. Chen, F.S. Zhang, Z.Y. Zhu, Isospin effects on rotational flow in intermediate energy heavy ion collisions. *Phys. Rev. C* **61**, 067601 (2000). <https://doi.org/10.1103/PhysRevC.61.067601>
25. V.N. Russkikh, Y.B. Ivanov, Collective flow in heavy-ion collisions for $E_{lab}=1\text{--}160$ GeV/nucleon. *Phys. Rev. C* **74**, 034904 (2006). <https://doi.org/10.1103/PhysRevC.74.034904>
26. Z.Q. Feng, Dynamics of strangeness and collective flows in heavy-ion collisions near threshold energies. *Nucl. Phys. A* **919**, 32 (2013). <https://doi.org/10.1016/j.nuclphysa.2013.10.005>
27. S. Gautam, A.D. Sood, R.K. Puri et al., Isospin effects in the disappearance of flow as a function of colliding geometry. *Phys. Rev. C* **83**, 014603 (2011). <https://doi.org/10.1103/PhysRevC.83.014603>
28. T.Z. Yan, Y.G. Ma, X.Z. Cai et al., Scaling of anisotropic flows and nuclear equation of state in intermediate energy heavy ion collisions. *Chin. Phys.* **16**(9), 2676–2682 (2007). <https://doi.org/10.1088/1009-1963/16/9/031>
29. T.Z. Yan, S. Li, Y.N. Wang et al., Yield ratios and directed flows of light particles from proton-rich nuclei-induced collisions. *Nucl. Sci. Tech.* **30**, 15 (2019). <https://doi.org/10.1007/s41365-018-0534-6>
30. B. Gao, Y.J. Wang, Q.F. Li et al., Influence of Fermi momentum on elliptic flow in heavy-ion collisions at intermediate energies. *Nucl. Tech. (in Chinese)* **46**(07), 070501 (2023). <https://doi.org/10.11889/j.0253-3219.2023.hj.46.070501>
31. J.Y. Liu, Q. Zhao, S.J. Wang et al., Entrance channel dependence and isospin dependence of preequilibrium nucleon emission in intermediate energy heavy ion collisions. *Nucl. Phys. A* **687**, 475 (2001). [https://doi.org/10.1016/S0375-9474\(00\)00581-9](https://doi.org/10.1016/S0375-9474(00)00581-9)
32. X.C. Zhang, B.A. Li, L.W. Chen et al., Impact parameter dependence of the double neutron/proton ratio of nucleon emissions in isotopic reaction systems. *Chin. Phys. Lett.* **26**(5), 052502 (2009). <https://doi.org/10.1088/0256-307X/26/5/052502>
33. H.L. Liu, G.C. Yong, D.H. Wen, Probing the momentum dependence of the symmetry potential by the free n/p ratio of pre-equilibrium emission. *Phys. Rev. C* **91**, 024604 (2015). <https://doi.org/10.1103/PhysRevC.91.024604>
34. D. Thériault, J. Gauthier, F. Grenier et al., Neutron-to-proton ratios of quasiprojectile and midrapidity emission in the $^{64}\text{Zn} + ^{64}\text{Zn}$ reaction at 45 MeV/nucleon. *Phys. Rev. C* **74**, 051602(R) (2006). <https://doi.org/10.1103/PhysRevC.74.051602>
35. Y.X. Zhang, M.B. Tsang, Z.X. Li et al., Constraints on nucleon effective mass splitting with heavy ion collisions. *Phys. Lett. B* **732**, 186–190 (2014). <https://doi.org/10.1016/j.physletb.2014.03.030>
36. W.J. Xie, J. Su, L. Zhu et al., Neutron-proton effective mass splitting in a Boltzmann-Langevin approach. *Phys. Rev. C* **88**, 061601(R) (2013). <https://doi.org/10.1103/PhysRevC.88.061601>
37. J. Su, L. Zhu, C.Y. Huang et al., Correlation between symmetry energy and effective κ -mass splitting with an improved isospin- and momentum-dependent interaction. *Phys. Rev. C* **94**, 034619 (2016). <https://doi.org/10.1103/PhysRevC.94.034619>
38. X.Y. Sun, D.Q. Fang, Y.G. Ma et al., Neutron/proton ratio of nucleon emissions as a probe of neutron skin. *Phys. Lett. B* **682**, 396–400 (2010). <https://doi.org/10.1016/j.physletb.2009.11.031>
39. D.Q. Fang, Neutron skin thickness and its effects in nuclear reactions. *Nucl. Tech. (in Chinese)* **46**(08), 080016 (2023). <https://doi.org/10.11889/j.0253-3219.2023.hj.46.080016>
40. Z.T. Dai, D.Q. Fang, Y.G. Ma et al., Triton/ ^3He ratio as an observable for neutron-skin thickness. *Phys. Rev. C* **89**, 014613 (2014). <https://doi.org/10.1103/PhysRevC.89.014613>
41. W.J. Xie, F.S. Zhang, Probing the density dependence of the symmetry energy with central heavy ion collisions. *Nucl. Sci. Tech.* **24**(5), 050502 (2013). <https://doi.org/10.13538/j.1001-8042/nst.2013.05.002>
42. X.Q. Liu, M.R. Huang, W.P. Lin et al., Symmetry energy extraction from primary fragments in intermediate heavy-ion collisions. *Nucl. Sci. Tech.* **26**(2), S20508 (2015). <https://doi.org/10.13538/j.1001-8042/nst.26.S20508>
43. Z.Q. Feng, Nuclear dynamics and particle production near threshold energies in heavy-ion collisions. *Nucl. Sci. Tech.* **29**(3), 40 (2018). <https://doi.org/10.1007/s41365-018-0379-z>
44. T.Z. Yan, S. Li, Impact parameter dependence of the yield ratios of light particles as a probe of neutron skin. *Nucl. Sci. Tech.* **30**, 43 (2019). <https://doi.org/10.1007/s41365-019-0572-8>
45. T.Z. Yan, S. Li, Yield ratios of light particles as a probe of the proton skin of a nucleus and its centrality dependence. *Phys. Rev. C* **101**, 054601 (2020). <https://doi.org/10.1103/PhysRevC.101.054601>
46. D. Vautherin, D.M. Brink, Hartree-Fock calculations with Skyrme's interaction. I. Spherical. *Nucl. Phys. Rev. C* **5**, 626 (1972). <https://doi.org/10.1103/PhysRevC.5.626>
47. J. Aichelin, "Quantum" molecular dynamics—a dynamical microscopic n-body approach to investigate fragment formation and the nuclear equation of state in heavy ion collisions. *Phys. Rep.* **202**, 233–360 (1991). [https://doi.org/10.1016/0370-1573\(91\)90094-3](https://doi.org/10.1016/0370-1573(91)90094-3)
48. S.Q. Zhang, J. Meng, S.G. Zhou, Proton magic even-even isotopes and giant halos of Ca isotopes with relativistic continuum Hartree-Bogoliubov theory. *Sci. in Chin. (Series G)* **46**(6), 632–658 (2003). <https://doi.org/10.1360/03yw0140>
49. P. Sarriguren, M.K. Gaidarov, E.M. de Guerra et al., Nuclear skin emergence in Skyrme deformed Hartree-Fock calculations. *Phys.*

- Rev. C **76**, 044322 (2007). <https://doi.org/10.1103/PhysRevC.76.044322>
50. M. Warda, X. Viñas, X. Roca-Maza et al., Analysis of bulk and surface contributions in the neutron skin of nuclei. Phys. Rev. C **81**, 054309 (2010). <https://doi.org/10.1103/PhysRevC.81.054309>
51. J. Liu, C. Gao, N. Wan et al., Basic quantities of the Equation of State in isospin asymmetric nuclear matter. Nucl. Sci. Tech. **32**(11), 117 (2021). <https://doi.org/10.1007/s41365-021-00955-2>

Springer Nature or its licensor (e.g. a society or other partner) holds exclusive rights to this article under a publishing agreement with the author(s) or other rightsholder(s); author self-archiving of the accepted manuscript version of this article is solely governed by the terms of such publishing agreement and applicable law.